Kinetic modeling of hyperpolarized $^{13}C_1$-pyruvate metabolism in normal rats and TRAMP mice

Matthew L. Zierhut [a,b], Yi-Fen Yen [c], Albert P. Chen [b], Robert Bok [b], Mark J. Albers [a,b], Vickie Zhang [b], Jim Tropp [c], Ilwoo Park [a,b], Daniel B. Vigneron [a,b], John Kurhanewicz [a,b], Ralph E. Hurd [c], Sarah J. Nelson [a,b,*]

[a] *UCSF/UCB Joint Graduate Group in Bioengineering, San Francisco, CA, United States*
[b] *UCSF Surbeck Laboratory of Advanced Imaging, Department of Radiology and Biomedical Imaging, San Francisco, CA, United States*
[c] *Global Applied Sciences Laboratory, GE Healthcare, CA, United States*

ARTICLE INFO

ABSTRACT

Purpose: To investigate metabolic exchange between $^{13}C_1$-pyruvate, $^{13}C_1$-lactate, and $^{13}C_1$-alanine in pre-clinical model systems using kinetic modeling of dynamic hyperpolarized ^{13}C spectroscopic data and to examine the relationship between fitted parameters and dose–response.
Materials and methods: Dynamic ^{13}C spectroscopy data were acquired in normal rats, wild type mice, and mice with transgenic prostate tumors (TRAMP) either within a single slice or using a one-dimensional echo-planar spectroscopic imaging (1D-EPSI) encoding technique. Rate constants were estimated by fitting a set of exponential equations to the dynamic data. Variations in fitted parameters were used to determine model robustness in 15 mm slices centered on normal rat kidneys. Parameter values were used to investigate differences in metabolism between and within TRAMP and wild type mice.
Results: The kinetic model was shown here to be robust when fitting data from a rat given similar doses. In normal rats, Michaelis–Menten kinetics were able to describe the dose–response of the fitted exchange rate constants with a 13.65% and 16.75% scaled fitting error (SFE) for $k_{pyr \to lac}$ and $k_{pyr \to ala}$, respectively. In TRAMP mice, $k_{pyr \to lac}$ increased an average of 94% after up to 23 days of disease progression, whether the mice were untreated or treated with casodex. Parameters estimated from dynamic ^{13}C 1D-EPSI data were able to differentiate anatomical structures within both wild type and TRAMP mice.
Conclusions: The metabolic parameters estimated using this approach may be useful for *in vivo* monitoring of tumor progression and treatment efficacy, as well as to distinguish between various tissues based on metabolic activity.

1. Introduction

The biochemical processes observed in cancerous tissue may be markedly different than those in anatomically similar normal tissue [1,2]. A number of such processes have been investigated using *in vivo* ^{13}C magnetic resonance spectroscopy (MRS) and mathematical modeling, but have suffered from relatively low signal to noise ratios [3,4]. With the recent development of dynamic nuclear polarization (DNP) it has been possible to increase the ^{13}C MR signal intensity by more than 10,000-fold [5] and to provide dramatic improvements in the ability to study *in vivo* ^{13}C metabolism [6–10].

Pyruvate is an important end product of glycolysis that is preferentially converted in the mitochondria of healthy cells to acet-yl-CoA and carbon dioxide via pyruvate dehydrogenase (PDH). Acetyl-CoA enters the tricarboxylic acid (TCA) cycle and eventually provides cellular energy as ATP. Without oxygen, or if the TCA cycle is running at full capacity, healthy tissue is forced to maintain energy needs through an alternate pathway that converts pyruvate to lactate via lactate dehydrogenase (LDH) and oxidizes NADH to NAD^+. The NAD^+ is then available to aid in further glycolytic conversion of glucose to pyruvate, providing cellular energy as ATP. Another common pathway for pyruvate is conversion to alanine via alanine transaminase (ALT), which is known to occur in healthy liver and sometimes muscle. Fig. 1 shows a simplified diagram of these biochemical pathways that follows the C_1 carbon of pyruvate.

There are a number of changes in the metabolic products of pyruvate that may be of interest for the evaluation of tumors. One key finding is that all tumors preferentially undergo conversion of pyruvate to lactic acid, even in the presence of oxygen. This observation is known as aerobic glycolysis, or the Warburg effect [11,12]. Some cancer cells also show changes in transaminase

* Corresponding author. Address: UCSF/UCB Joint Graduate Group in Bioengineering, University of California, San Francisco, P.O. Box 2532, QB3 Bldg, 1700 4th Street, San Francisco, CA 94143-2532, United States. Fax: +1 415 514 2550.
E-mail address: Sarah.Nelson@radiology.ucsf.edu (S.J. Nelson).
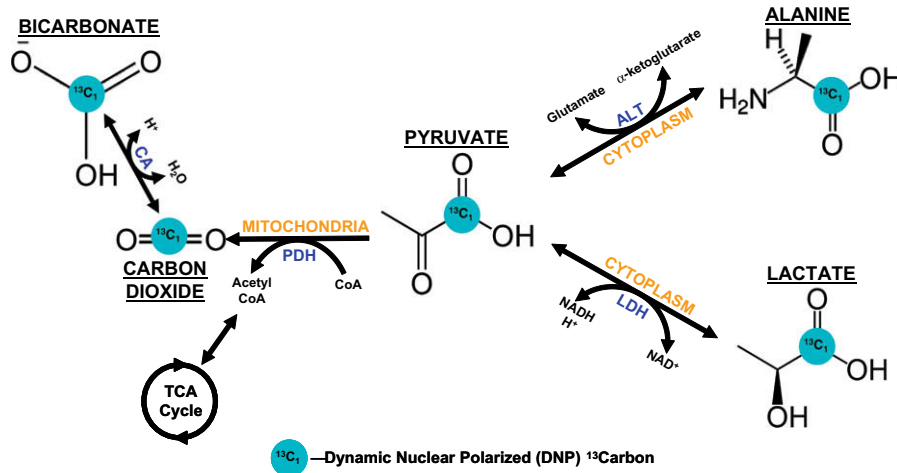
Fig. 1. Simplified diagram of the biochemical pathways taken by $^{13}C_1$-pyruvate that are visible with the hyperpolarized MR spectroscopy techniques discussed here. The position of the hyperpolarized ^{13}C nucleus is shown in all metabolites with the 🔵 $^{13}C_1$ symbol. LDH = lactate dehydrogenase. PDH, pyruvate dehydrogenase complex. ALT, alanine transaminase. CA, carbonic anhydrase.

activity, suggesting pyruvate-to-alanine exchange may be enhanced or suppressed, depending on tumor type [13–16]. Therefore, it may be possible to discern healthy tissue from cancerous tissue or to monitor cancer progression by injecting ^{13}C-pyruvate and monitoring the changes in ^{13}C-lactate, ^{13}C-alanine, and/or the MR signals from other metabolic products.

Prostate cancer is the most prevalent form of cancer in men, making up approximately 25% of all new male cancer diagnoses each year in the US [17]. A transgenic model of prostate cancer in mice (TRAMP) has been developed for its similarities to human prostate cancer, in that the tumor occurs spontaneously and follows a similar pattern of progression [18]. By studying the TRAMP model using hyperpolarized ^{13}C techniques, important details about prostate cancer may be learned, with future studies aimed at investigating other tumor types and cancer in general.

This study uses dynamic MRS data to investigate $^{13}C_1$-pyruvate metabolism in healthy rats and mice, and in TRAMP mice. This agent was chosen because of the relatively long T_1 value of the ^{13}C nucleus in the C_1 position. Simple exponential equations were used to model the dynamic changes in $^{13}C_1$-pyruvate, $^{13}C_1$-lactate, and $^{13}C_1$-alanine levels following a bolus of the hyperpolarized agent. The goal of the study was to use a range of different doses of hyperpolarized $^{13}C_1$-pyruvate in order to assess the dose–response and to investigate whether it could be modeled with Michaelis–Menten-like kinetics.

2. Methods

Twelve healthy male Sprague–Dawley rats (median mass of 330 g) were injected with hyperpolarized $^{13}C_1$-pyruvate through a tail vein catheter. Two male wild type and ten TRAMP mice (median mass of 35.5 g) were injected with hyperpolarized $^{13}C_1$-pyruvate through a jugular vein catheter. The TRAMP mice were serially studied to monitor tumor progression and treatment response, whereas healthy rats and mice were sacrificed immediately after imaging. The TRAMP mice received up to 12 $^{13}C_1$-pyruvate injections over multiple studies and the healthy mice and rats received a maximum of three $^{13}C_1$-pyruvate injections. Imaging and spectroscopy were performed on a GE 3T MR scanner (GE Healthcare, Waukesha, WI) with a dual-tuned ($^{1}H/^{13}C$) quadrature coil, either customized for rats (8 cm inner diameter, 9 cm length, sensitive volume: 75 mm diameter and 90 mm length) or customized for mice (5 cm inner diameter,
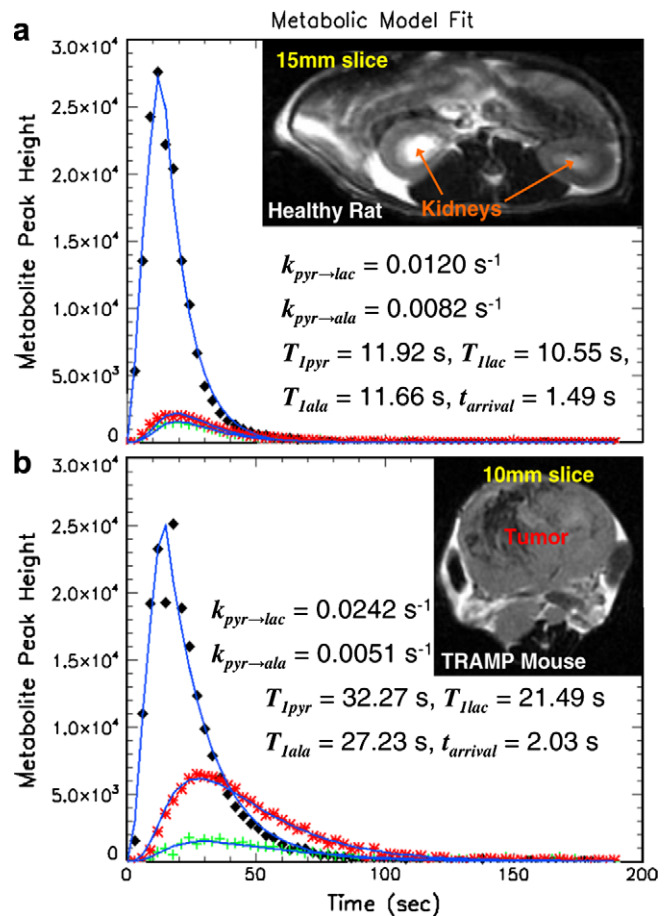
Fig. 2. Examples of dynamic curves of metabolite levels in a 15 mm slice centered on healthy rat kidney (a) and a 10 mm slice centered on TRAMP tumor (b). Pyruvate data are represented by black diamonds (♦), lactate data are represented by red asterisks (∗), alanine data are represented by green plus signs (+), and the estimated best fit lines are represented by the blue lines. Metabolic parameters, estimated from the model in equations 1 and 2 are also listed inside their respective plots, along with a T_2 fast spin-echo (FSE) ^{1}H image of the slice used to acquire ^{13}C data. Both animals received a dose of approximately 725 μmol/kg of hyperpolarized $^{13}C_1$-pyruvate injected over 12 s.

8 cm length) [7]. The specifics of the animal handling procedure have been reported previously [7,19]. All experiments were conducted under a protocol approved by our institutional animal care and use committee.

Hyperpolarized $^{13}C_1$-pyruvate was generated with either a prototype DNP polarizer [19] or a Hypersense® system (Oxford Instruments, Abingdon, UK). Polarization levels ranged from 16% to 23%. Animals were given a range of pyruvate concentrations and volumes to assess the effects of dose on metabolite exchange. Rats received $^{13}C_1$-pyruvate at concentrations of 9.6–80 mM with volumes of 1.0–3.4 mL, yielding a $^{13}C_1$-pyruvate dose between 28.1 and 724.2 μmol/kg. In TRAMP and wild type mice, doses ranged from 92.4 to 857.9 μmol/kg (10–80 mM, 300–400 μL). The injections lasted between 4 and 13 s in rats, but were consistently 12 s in the mice.

In 12 of the rats (21 scans), dynamic spectroscopy data were acquired from a single 15 mm axial slice centered on the kidneys (Flip angle = 5°, spectral bandwidth (BW) = 5 kHz, 2048 spectral points) using a spin-echo RF pulse sequence. Data acquisition began simultaneously with the $^{13}C_1$-pyruvate injection and was repeated every 3 s (TR = 3 s) over a duration of 189 s (64 time points). The same acquisition was used for six TRAMP mice (11 scans) with a 10 mm axial slice centered on the primary tumor in the prostate. Chemical shift mis-registration between pyruvate and lactate for the 2.8 kHz hyperbolic secant RF selection pulses [7] was estimated at approximately 2 mm for the 15 mm slice selection and 1.4 mm for the 10 mm slice selection. Volumes of tumor that were estimated to be within the observed 10 mm slices ranged from approximately 0.6–3.2 cc.

A one-dimensional flyback echo-planar spectroscopic imaging (1D-EPSI) technique was used to acquire dynamic data in two healthy wild type mice (3 scans) and five TRAMP mice (15 scans) [20]. The readout gradient was applied in the superior–inferior (SI) dimension during acquisition to allow spatial encoding with a 10 mm slice resolution and a 160 mm field of view (FOV). The readout trajectory was designed for a spectral bandwidth of 581.4 Hz with 288 spectral points [21]. The other acquisition parameters remained the same.

High-resolution T_2-weighted anatomical ^1H images were acquired to reference the spectroscopic data in both rats and mice. Acquisition details for these images have been published previously [7,9,19].

Data were processed using an algorithm that was implemented in the Interactive Data Language (IDL, ITT Visual Information Solutions, Boulder, CO). For the single slice data, a 10 Hz Lorentzian apodization was applied to each free-induction decay (FID) prior to Fourier transforming the data. Zero-order phasing was applied to maximize the value of the first point in the FID. The average baseline signal was then subtracted and the real peak heights for $^{13}C_1$-pyruvate, $^{13}C_1$-lactate, and $^{13}C_1$-alanine were used as input data for the models described below. The 1D-EPSI data were processed similarly, with additional phase corrections to account for the time delays in the FID that result from the spatial encoding [22]. These data were zero-filled spatially in the SI dimension to 1.25 mm resolution in order to more precisely reference the metabolite levels to specific tissues.

A model for the change in $^{13}C_1$-pyruvate signal over time was first fit to the pyruvate peak height data according to the following piecewise equation:

$$M_{pyr}(t) = \begin{cases} \frac{rate_{inj}}{k_{pyr}}\left(1 - e^{-k_{pyr}(t-t_{arrival})}\right), & t_{arrival} \leqslant t < t_{end} \\ M_{pyr}(t_{end})e^{-k_{pyr}(t-t_{end})}, & t \geqslant t_{end} \end{cases}$$

(1)

where $M_{pyr}(t)$ represents $^{13}C_1$-pyruvate peak height as a function of time. The parameters fit by this model are: k_{pyr}, the rate constant for

pyruvate signal decay (in s^{-1}); $rate_{inj}$, the rate of pyruvate arrival (in a.u. s^{-1}); and $t_{arrival}$, the time of pyruvate arrival (in s). The signal was assumed to be zero for all metabolites prior to $t_{arrival}$. The variable, t_{end}, can be calculated as the sum of the fitted arrival time, $t_{arrival}$, and the known injection duration. The three estimated pyruvate parameters (k_{pyr}, $rate_{inj}$, $t_{arrival}$) were then used to fit the following equation with $^{13}C_1$-lactate and $^{13}C_1$-alanine dynamic data:

$$M_x(t) = \begin{cases} \frac{k_{pyr \to x}rate_{inj}}{k_{pyr}-k_x}\left(\frac{1-e^{-k_x(t-t_{arrival})}}{k_x} - \frac{1-e^{-k_{pyr}(t-t_{arrival})}}{k_{pyr}}\right), & t_{arrival} \leqslant t < t_{end} \\ \frac{M_{pyr}(t_{end})k_{pyr \to x}}{k_{pyr}-k_x}\left(e^{-k_x(t-t_{end})} - e^{-k_{pyr}(t-t_{end})}\right) \\ \quad + M_x(t_{end})e^{-k_x(t-t_{end})}, & t \geqslant t_{end} \end{cases}$$

(2)

Here, x represents either lactate (lac) or alanine (ala), and $M_x(t)$ represents either $^{13}C_1$-lactate or $^{13}C_1$-alanine peak heights over time. Two parameters were estimated: $k_{pyr \to lac}$ (or $k_{pyr \to ala}$), the rate constant for pyruvate to lactate (or alanine) exchange (s^{-1}), and k_{lac} (or k_{ala}), the rate constant for lactate (or alanine) signal decay (s^{-1}). Metabolite signal decay rate constants (k_{pyr}, k_{lac}, and k_{ala}) were assumed to consist of both metabolite T_1 decay and signal loss from the 5° RF flip angles. This meant that T_1 values could be estimated for lactate and alanine after accounting for RF excitations and for pyruvate after also accounting for metabolic exchange rate constants. The robustness of parameter estimation was assessed based upon multiple scans on a healthy rat that was given three similar $^{13}C_1$-pyruvate doses (321.4–321.9 μmol/kg).

In addition to metabolism, T_1 effects, and RF excitations, all rate constants may be influenced by other sources of signal change or variation, and they should be thought of as apparent, rather than absolute, rate constants. Also note that reverse exchange of metabolites back to pyruvate was assumed to be negligible in this model to allow the estimation of irreversible Michaelis–Menten kinetics. This was further shown to be a reasonable assumption in previous studies that used hyperpolarized $^{13}C_1$-lactate as the injected substrate [23].

The dose effects were represented by a Michaelis–Menten-like model with maximum reaction velocity (V_{max}) and Michaelis constant (K_m) according to the following equation:

$$k_{pyr \to x} = \frac{V_{max}}{K_m + Dose_{pyr}}$$

(3)

The kinetics are described here using $k_{pyr \to lac}$ and $k_{pyr \to ala}$ instead of initial reaction rates (V_0). This modified Michaelis–Menten equation is simply the inverse of the Hanes–Woolf equation [24]. To adhere to the traditional Michaelis–Menten equation, the initial reaction rates (V_0) relative to pyruvate dose were also estimated as the product of dose ($Dose_{pyr}$) and exchange rate constants ($k_{pyr \to lac}$ and $k_{pyr \to ala}$). Parameter estimates from nineteen scans (11 rats) were used to fit Eq. (3) and estimate V_{max} and K_m for exchange with lactate and exchange with alanine. The robustness of the model fit was assessed via the scaled fitting error [25].

Metabolic parameters from ten TRAMP mouse tumors (26 scans) and two wild type mice (3 scans) were considered. In wild type mice, comparison data came from the region containing normal prostate. Three TRAMP mice underwent serial studies at a constant pyruvate dose (two with hormone deprivation treatment of casodex administered immediately after the first scan, one without treatment) to investigate how metabolic parameters change with disease progression. Tumor stage was assessed by size and appearance. Four TRAMP mice (two mid-stage tumors, two late-stage tumors) received a range of three $^{13}C_1$-pyruvate doses on studies performed within a short time period (7 days for one, 4 h for the other three); these data were used to separately fit Eq. (3) and to

Table 1
Reproducibility in the exchange parameters for a 15 mm slice centered on healthy rat kidney. Parameters are shown with standard error (±se) estimated from the covariance matrix of the model fitting.

Dose$_{pyr}$ (μmol/kg)	$k_{pyr \to lac} \pm$ se (s^{-1})	$k_{pyr \to ala} \pm$ se (s^{-1})
321.4	0.0235 ± 0.00041	0.0229 ± 0.00068
321.9	0.0217 ± 0.00072	0.0214 ± 0.00081
321.9	0.0255 ± 0.00052	0.0192 ± 0.00064
Mean	0.0236 ± 0.00055	0.0211 ± 0.00071

describe the individual dose–responses. Four TRAMP mice underwent only one dynamic spectroscopy scan.

3. Results

A normal rat that was given three similar doses of $^{13}C_1$-pyruvate showed highly reproducible parameter estimates (see Table 1). In nineteen scans, with doses ranging from 36 to 724 μmol/kg, the median *in vivo* T_1 estimates (±SD) in slices centered on normal rat kidney were 12.7 ± 4.4, 12.7 ± 1.7, and 12.1 ± 2.4 s for $^{13}C_1$-pyruvate, $^{13}C_1$-lactate, and $^{13}C_1$-alanine, respectively. Fig. 2a shows an example of dynamic curves of metabolite levels in a 15 mm slice

centered on healthy rat kidney for a dose of 725 μmol/kg, including parameter estimates.

Fig. 3 shows the Michaelis–Menten model fit and parameter estimates for $k_{pyr \to lac}$ and $k_{pyr \to ala}$ dose–response in the slice centered on rat kidney. For $k_{pyr \to lac}$, the estimated maximum reaction rate (V_{max}) was 11.12 ± 1.28 μmol/kg/s and the Michaelis constant (K_m) was 161.45 ± 30.03 μmol/kg. For $k_{pyr \to ala}$, V_{max} was 10.61 ± 1.77 μmol/kg/s and K_m was 279.55 ± 67.42 μmol/kg. SFE values were less than 20% for lactate (13.65%) and for alanine (16.75%). Traditional Michaelis–Menten curves are shown in Fig. 4 using the value of V_0 that was calculated from the product of Dose$_{pyr}$ and $k_{pyr \to lac}$ (or $k_{pyr \to ala}$).

Fig. 2b shows an example of dynamic curves in a 10 mm slice centered on TRAMP prostate tumor for a dose of 725 μmol/kg. The lactate curve is noticeably elevated compared to the results from the rat, thus elevating the estimated value of $k_{pyr \to lac}$. The estimated values of T_1 were also higher in the TRAMP mouse than in the rat. Metabolic parameters were estimated for a 10 mm slice centered on tumor in ten TRAMP mice (26 scans) to give median T_1 values (±SD) of 17.4 ± 2.8 s for $^{13}C_1$-lactate and 21.3 ± 6.5 s for $^{13}C_1$-alanine. In the five TRAMP mice and two wild type mice (18 total scans) for whom a dynamic 1D-EPSI acquisition was acquired, it was possible to estimate T_1 values in multiple axial slices. In the
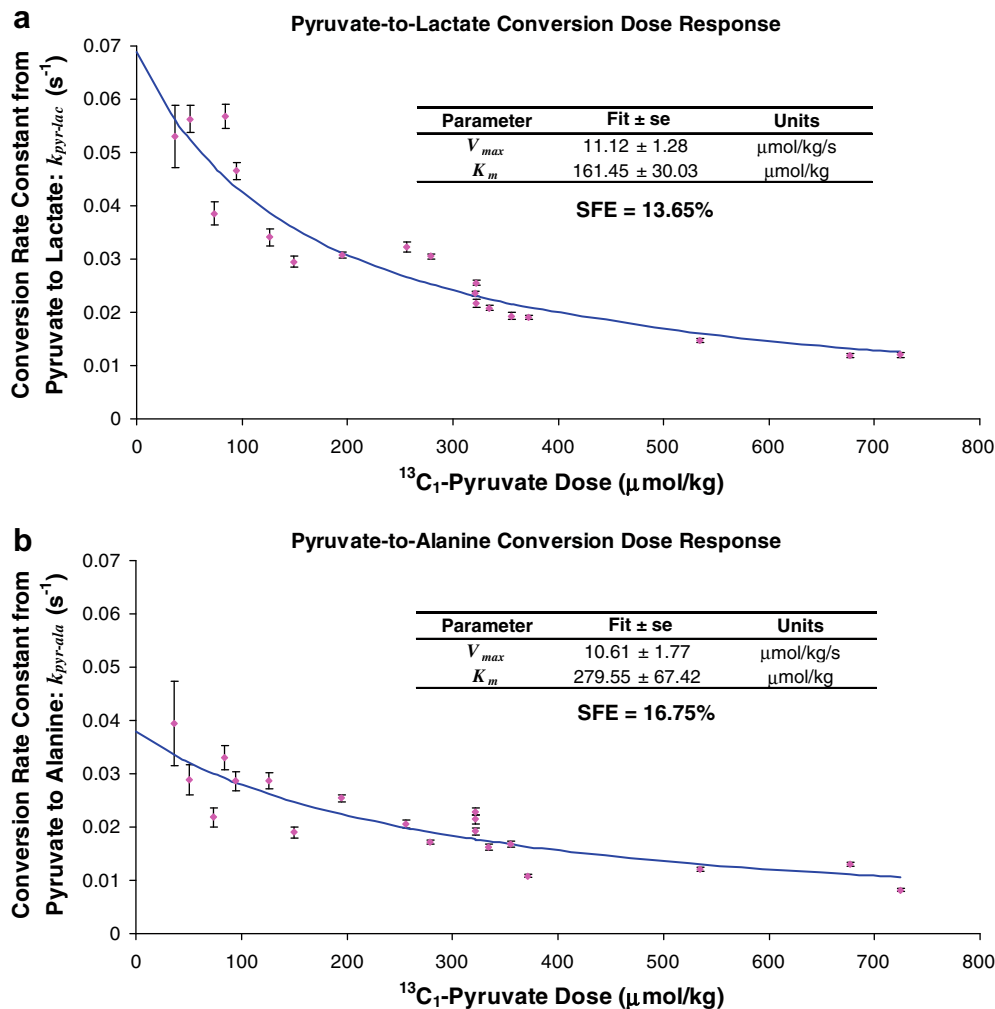
Fig. 3. Response of metabolic exchange parameters, $k_{pyr \to lac}$ (a) and $k_{pyr \to ala}$ (b), to varying doses of $^{13}C_1$-pyruvate. Data are represented by the pink circles (with ±standard error bars). Michaelis–Menten kinetic parameters (V_{max} and K_m) are listed in the inset tables with standard error (±se) estimated from the covariance matrix of the Michaelis–Menten model fitting. The blue line represents the Michaelis–Menten best fit. Scaled fitting error (SFE) is also shown to represent how well the Michaelis–Menten model fits the dose–response data.
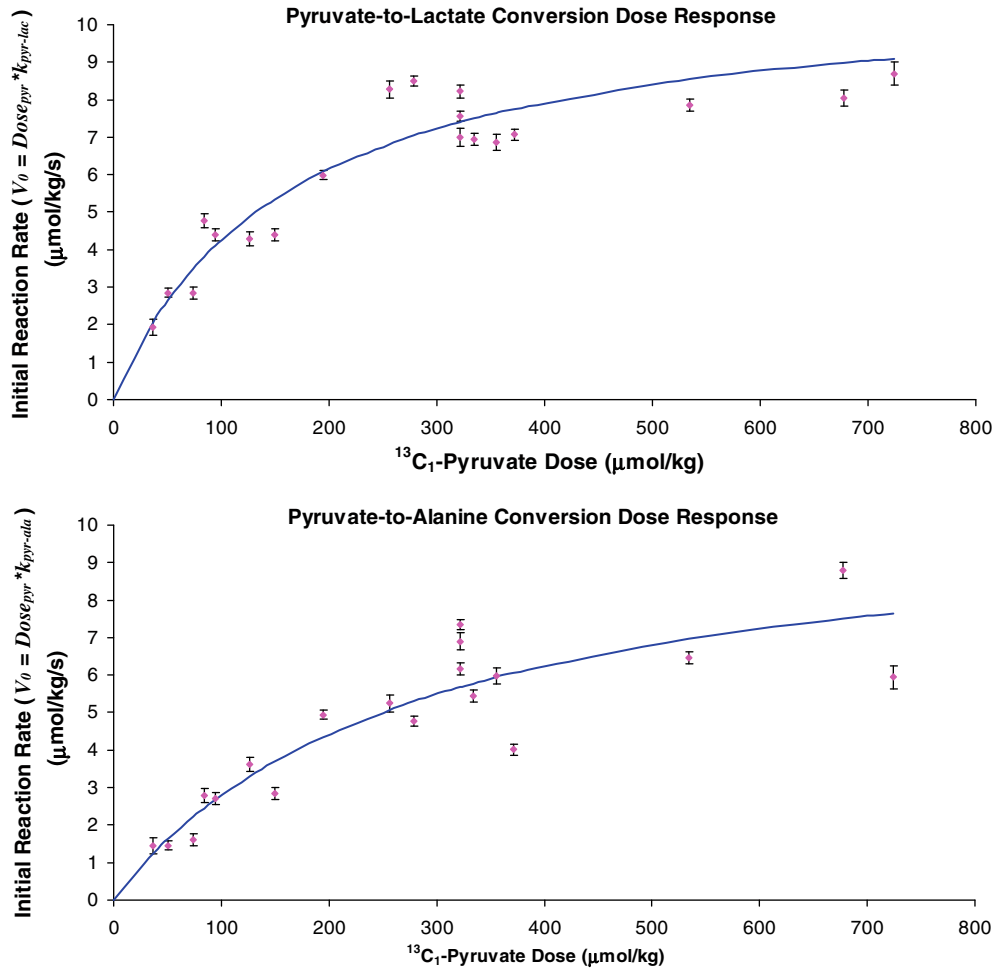
Fig. 4. Response of initial reaction rates (V_0) to varying doses of $^{13}C_1$-pyruvate. Values for V_0 were calculated as the product of $Dose_{pyr}$ and $k_{pyr\to lac}$ (a) and $Dose_{pyr}$ and $k_{pyr\to ala}$ (b). Error bars were calculated using error propagation (product of standard error of the estimated parameter and $Dose_{pyr}$). Michaelis–Menten kinetic parameters (V_{max} and K_m) from Fig. 2 were used to calculate the blue best fit line.
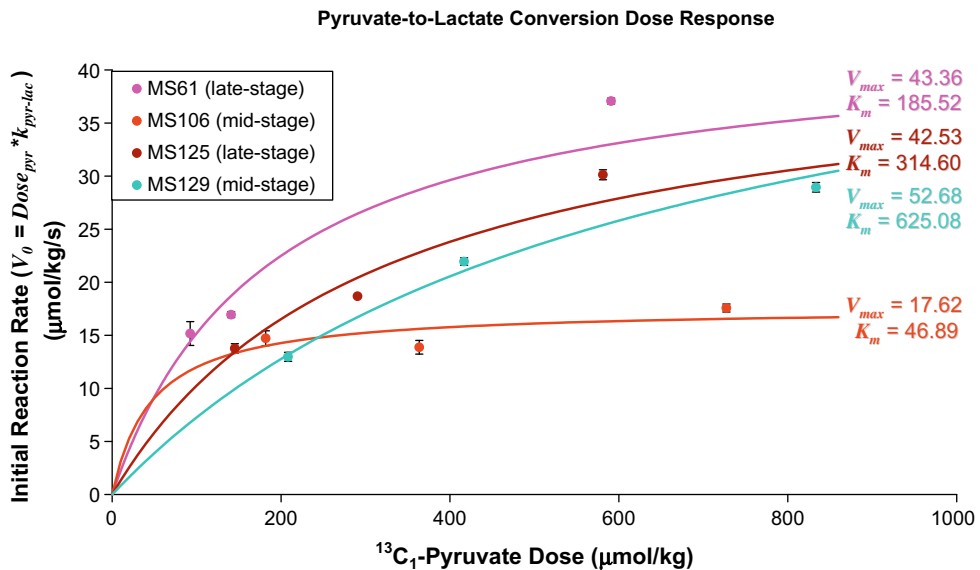
Fig. 5. Response of initial pyruvate to lactate reaction rates in four 10 mm slices containing TRAMP tumor to varying doses of $^{13}C_1$-pyruvate. All mice had developed a transgenic prostate tumor prior to these data acquisitions. Best fit estimates of Michaelis–Menten kinetic parameters are shown next to the best fit curves (V_{max} in μmol/kg/s, K_m in μmol/kg). MS61 (pink) received three injections spanning seven days. MS106 (red), MS125 (brown), and MS129 (cyan) all received three injections within a 4 h period. MS106 and MS129 were categorized as mid-stage tumors and MS61 and MS125 were categorized as late-stage tumors.

region containing mouse kidneys the median T_1 value for $^{13}C_1$-lactate was 10.4 ± 0.8 s and the median value for $^{13}C_1$-alanine was 6.5 ± 0.9 s. In mice, the T_1 values for $^{13}C_1$-pyruvate were highly variable.

Fig. 5 shows the dose–response in four TRAMP mice that were given three different $^{13}C_1$-pyruvate doses, ranging from 92 to 833 µmol/kg. MS61 (late-stage tumor) was given a range of doses over 1 week, while MS106 (mid-stage tumor), MS125 (late-stage tumor), and MS129 (mid-stage tumor) received all of the doses within the same exam (~4 h). All four mice exhibited a $k_{pyr \to lac}$ dose–response that could be represented by Michaelis–Menten kinetics. The late-stage tumors appeared to have similar dose–responses and V_{max} values (~43 µmol/kg/s). One of the mid-stage tumors (MS106) showed a noticeably lower dose–response curve ($V_{max} = 17.6$ µmol/kg/s), while the other mid-stage tumor (MS129) had a similar dose–response to the late-stage tumors ($V_{max} = 52.7$ µmol/kg/s).

Three TRAMP mice were studied serially for up to 23 days (11 total scans) and were given a dose of approximately 800 µmol/kg (727–858 µmol/kg). The untreated mouse (MS53) showed a large increase in $k_{pyr \to lac}$ in a 10 mm slice containing tumor over a 23 day period, with values for $k_{pyr \to lac}$ increasing by more than 76% (from 0.038 to 0.067 s^{-1}). Additionally, $k_{pyr \to ala}$ was fairly stable in the untreated mouse (decreased from 0.0058 to 0.0049 s^{-1}) and the ratio of $k_{pyr \to lac}:k_{pyr \to ala}$ increased by more than 109% (from 6.5 to 13.5). These metabolic parameter estimates are in agreement with similar estimates in lymphoma-bearing mice [10], as well as other experimental models [4,26]. The two other TRAMP mice that were studied serially (MS99 and MS106) were treated with hormone deprivation (casodex). The ratio of $k_{pyr \to lac}:k_{pyr \to ala}$ remained lower for the treated mice relative to the untreated mouse, but there did not appear to be a significant difference between the treated mice and the untreated mouse in any of the metabolic parameters. Fig. 6 shows how the metabolic exchange parameters changed over time in these mice. It should be noted that these are very preliminary data, which are meant to illustrate the potential for applying this modeling approach to assessing response to therapy rather than providing definitive assessments of the effects of hormone therapy.

Fig. 7 shows 1D-EPSI data collected from a wild type mouse (Fig. 7a–d) compared to a TRAMP mouse (Fig. 7e–h). In ten TRAMP mice (18 scans) that were given 300–400 µL of 80 mM $^{13}C_1$-pyruvate (median ± SD = 790 ± 96.7 µmol/kg) and two wild type mice (2 scans) given 350 µL of 80 mM $^{13}C_1$-pyruvate (815 ± 11.8 µmol/kg), there were significant differences in estimated $k_{pyr \to ala}$ values ($p < 0.02$) and $k_{pyr \to lac}:k_{pyr \to ala}$ ratios ($p < 0.003$) in the region containing the prostate or tumor, but no statistically significant difference in $k_{pyr \to lac}$ values ($p > 0.05$). In TRAMP mice that had varying levels of disease development, all $k_{pyr \to ala}$ values were lower and all $k_{pyr \to lac}:k_{pyr \to ala}$ ratios were higher compared to the two wild type mice in the same region. Median $k_{pyr \to lac}$ and $k_{pyr \to ala}$ values (±SD) for TRAMP mice were 0.044 ± 0.012 s^{-1} and 0.0075 ± 0.0022 s^{-1}, ranging from 0.024 to 0.072 s^{-1} and 0.0028 to 0.011 s^{-1}, respectively. Median $k_{pyr \to lac}:k_{pyr \to ala}$ ratios (±SD) were 5.7 ± 3.8, ranging from 4.1 to 17.0. The two wild type mice showed values for $k_{pyr \to lac}$, $k_{pyr \to ala}$, and $k_{pyr \to lac}:k_{pyr \to ala}$ ranging from 0.029 to 0.047 s^{-1}, 0.012 to 0.013 s^{-1}, and 2.6 to 3.6, in the region containing the prostate. Additionally, differences in metabolic parameters between anatomical structures were present, and examples of this can be easily seen in Fig. 7.

4. Discussion

This study demonstrates the application of kinetic modeling to the *in vivo* changes in $^{13}C_1$-pyruvate, lactate, and alanine in Spra-
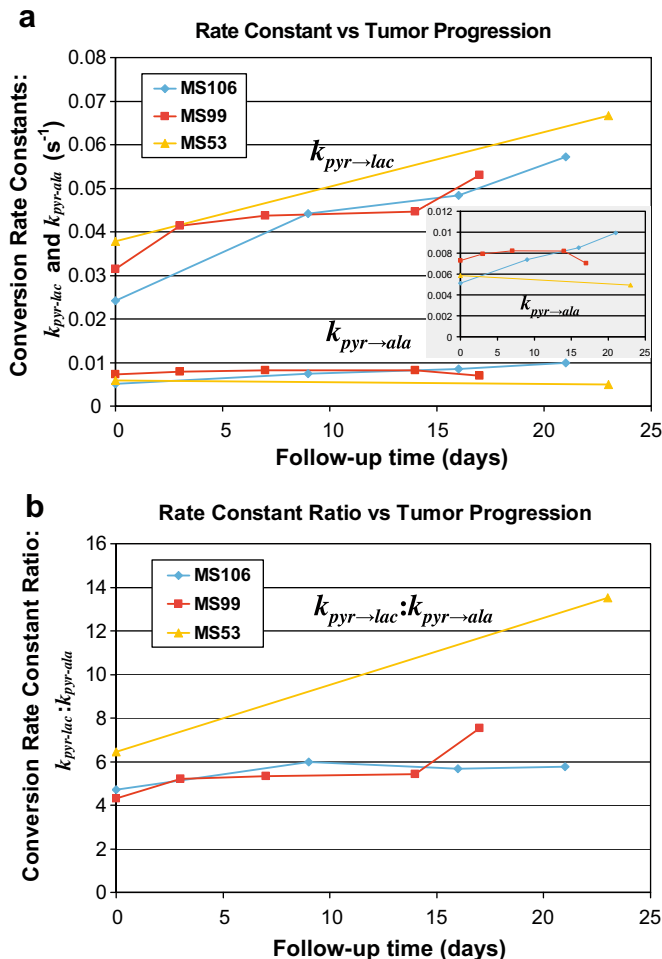

Fig. 6. Serial plots of estimated metabolic exchange parameters ($k_{pyr \to lac}$ and $k_{pyr \to ala}$) over time (a) and their ratios ($k_{pyr \to lac}:k_{pyr \to ala}$) over time (b) for three mice with a transgenic prostate tumor. A rescaled plot of $k_{pyr \to ala}$ is also shown (a). One mouse (MS53) was untreated, while two mice (MS99 and MS106) were treated with hormone deprivation (casodex). $k_{pyr \to lac}$ values appear to increase over time in all animals; however, $k_{pyr \to lac}:k_{pyr \to ala}$ values appear stable over time for treated animals, while $k_{pyr \to lac}:k_{pyr \to ala}$ more than doubles in the untreated animal over a 23 day period.

gue–Dawley rats, wild type mice, and TRAMP mice. The parameters estimated by this analysis appear to be robust but are highly dependent on $^{13}C_1$-pyruvate dose, as well as tissue type and disease state. When using hyperpolarized $^{13}C_1$-pyruvate to investigate differences in metabolic activity for various tissues, it is therefore critical to measure the time course of changes that are observed and also to take dose into account.

The variation in estimated parameters when conducting three identical studies on a rat was minimal. The T_1 estimates in slices centered on rat kidneys were in agreement with previously published values obtained from the whole rat [8]. A robust fit to the dose–response was achieved with a Michaelis–Menten-like model (SFE < 20%) in nineteen scans from rats. While it is clear that more complex models, which include corrections for the effects of diffusion, flow and multi-exponential decay, could be considered for future studies, the results that we have obtained suggest that the model used here is a robust option, which may be valuable for comparing ^{13}C metabolism in serial studies of treatment response and in other model systems.

The assumption of negligible reverse exchange from lactate and alanine back to pyruvate was consistent with the results obtained in our group using hyperpolarized ^{13}C-lactate as the substrate [23].
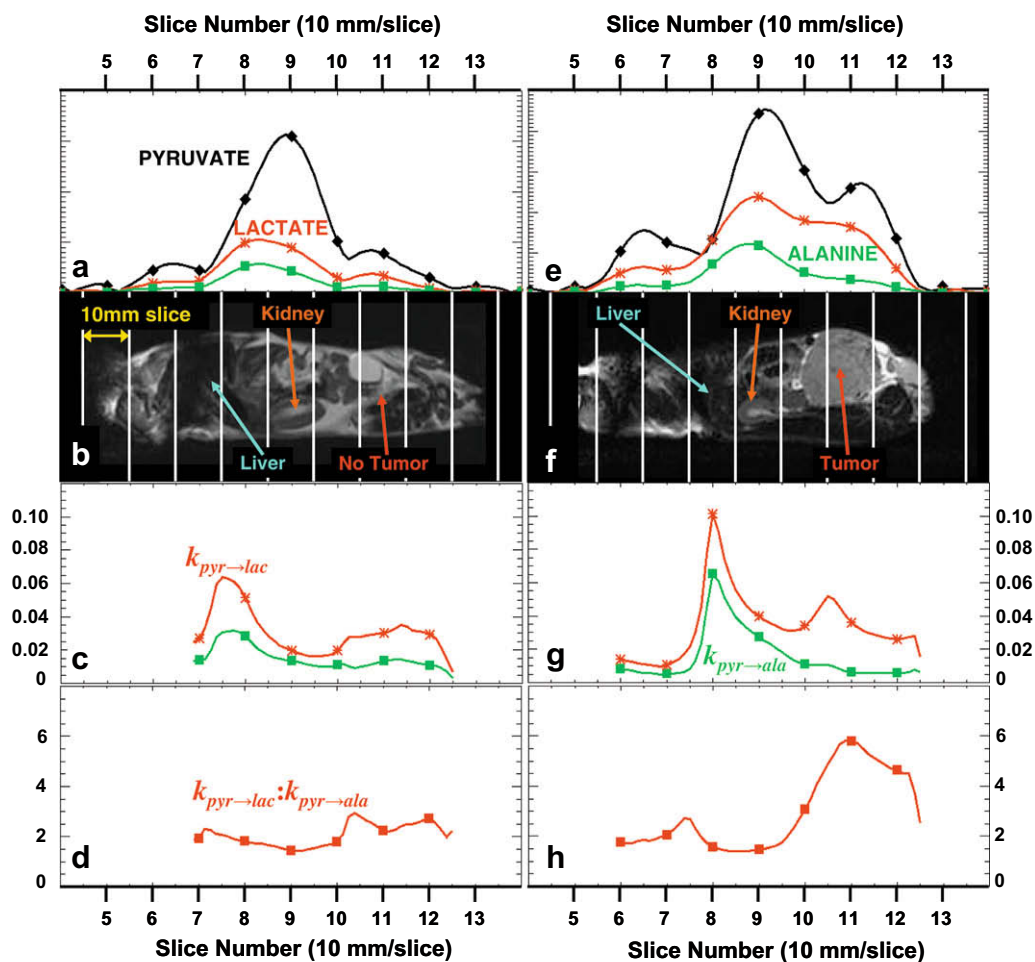
Fig. 7. One dimensional flyback echo-planar spectroscopic imaging (1D-EPSI) data from a wild type mouse (a–d) and a TRAMP mouse (e–h), each receiving 300–350 μL of 80 mM hyperpolarized $^{13}C_1$-pyruvate. Spectroscopic data was zero-filled in the SI dimension to eight times the acquired resolution. (a) and (e) show the metabolite signal along the superior-inferior (SI) dimension between 27 and 30 s post injection acquired for pyruvate (black), lactate (red), and alanine (green), with arbitrary units. (b) and (f) are sagittal T_2 FSE images that show the anatomical structures located within each 10 mm slice. Kidneys, liver, and tumor (or "no tumor") are labeled with colored arrows. (c) and (g) show $k_{pyr \to lac}$ (red) and $k_{pyr \to ala}$ (green), in s^{-1}, along the SI dimension in the healthy mouse (c) and TRAMP mouse (g). (d) and (h) show the ratios of metabolic exchange parameters along the SI dimension. There are noticeable differences between the TRAMP and healthy mice, as well as between their anatomical structures.

While some circumstances may require the use of a model employing bi-directional exchange, the relatively large quantity of pyruvate injected, the short time frame in which data are acquired, and the use of Michaelis–Menten kinetics favor the application of this more simplistic representation for these data. The estimated metabolic parameters reported here for slices containing TRAMP tumor are in good agreement with similar estimates in lymphoma-bearing mice that used a bi-directional exchange model [10]. Additionally, all the reported metabolic parameters do not conflict with other non-hyperpolarized NMR studies [4,26].

The TRAMP mouse model that was included in this study is representative of human prostate cancer, in that the tumors occur spontaneously and follow a similar pattern of progression. Single slice dynamic ^{13}C spectroscopy was applied to demonstrate the potential for assessing dose–response and for monitoring tumor progression and treatment effects. The 1D-EPSI technique was equally effective at monitoring dose–response and disease state with the added advantage of being able to show differences in anatomy within multiple slices from the animal.

Serial studies on three TRAMP mice showed how kinetic modeling of dynamic ^{13}C spectroscopy may be valuable in monitoring disease state. One of the TRAMP mice was untreated, and the estimated metabolic parameters showed a noticeable change which was much larger than the reproducibility error observed in rats. The 76% increase in $k_{pyr \to lac}$ and the 109% increase in $k_{pyr \to lac}:k_{pyr \to ala}$ may therefore be attributed to tumor progression, suggesting that TRAMP tumors produce more lactate in later stages. The two TRAMP mice that were treated with hormone deprivation (casodex) showed similar progression in $k_{pyr \to lac}$ with values that continually increased with each exam but the $k_{pyr \to lac}:k_{pyr \to ala}$ values appeared to be relatively stable (CV = 10% and 21%). If tumor volume was used as a measure of tumor progression, the prostate tumors in the two treated animals did not seem to progress as aggressively as the untreated mouse. However, this is a heterogeneous model of prostate cancer, and it is not clear if hormone deprivation or phenotype was responsible for slower growth. The model technique described in this paper will be valuable in future serial studies of response to therapy.

In the region containing prostate, the estimated pyruvate-to-alanine exchange rate constants ($k_{pyr \to ala}$) were lower in TRAMP mice and the ratio of rate constants ($k_{pyr \to lac}:k_{pyr \to ala}$) were higher compared to wild type mice who received a similar dose of approximately 800 μmol/kg. In an earlier 2D ^{13}C spectroscopic imaging study, Golman, et al. showed high lactate with low alanine levels in engrafted rat tumors, but the opposite in normal skeletal muscle [6]. These results suggest that the exchange of pyruvate with lactate may not only increase in tumors, but that it may increase more significantly relative to pyruvate-to-alanine exchange.

T_1 values for $^{13}C_1$-lactate and $^{13}C_1$-alanine that were estimated in slices containing TRAMP prostate tumor were on average higher compared to slices containing TRAMP mouse kidney and normal mouse and rat kidney. The T_1 values for $^{13}C_1$-pyruvate were quite variable in these regions, which may be attributed to the form of the expression used to fit the function and the fact that it requires correction for multiple metabolic exchange rate constants. The T_1 values for $^{13}C_1$-lactate and alanine are obtained from a simpler equation and were less variable. The range of metabolite T_1 values that were observed using 1D-EPSI suggests that there are distinct T_1 values for lactate, alanine, and pyruvate in various tissues. The estimated arrival time ($t_{arrival}$) also varied throughout the mouse anatomy, with the earliest arrival times being near the upper abdomen and heart.

Differences in estimated metabolic parameters were observed in different anatomical regions (Fig. 7). Slices containing kidneys in wild type and TRAMP mice produced the largest signal, while slices containing liver appeared to produce relatively low signal but exhibited the highest metabolic exchange rate constants. While the slice selection profiles and spatial encoding point spread function allow for some mis-registration and signal overlap, the large variations in the observed signals suggest that the changes observed are indeed physiologic in nature. This suggests that anatomy is a determinant of metabolic behavior and that these metabolic differences can be measured with hyperpolarized ^{13}C techniques. Studies are underway to investigate variations in metabolism across anatomical regions using 2D and 3D dynamic spectroscopic imaging protocols which will more accurately describe distinct metabolic activity in specific tissue types [27].

5. Conclusion

This study applied a kinetic model of changes in ^{13}C metabolism to analyze dynamic *in vivo* spectroscopy of murine systems. As expected from Michaelis–Menten kinetic theory, the substrate dose had a critical influence on metabolic parameters. The parameters estimated using this approach may be useful for monitoring tumor progression and treatment efficacy, as well as for distinguishing metabolic activity among different tissues.

Acknowledgment

References

[1] B.D. Ross, The biochemistry of living tissues: examination by MRS, NMR Biomed. 5 (5) (1992) 215–219. Review.

[2] M.I. Koukourakis, A. Giatromanolaki, E. Sivridis, K.C. Gatter, A.L. Harris, Tumor and Angiogenesis Research Group, Pyruvate dehydrogenase and pyruvate dehydrogenase kinase expression in non small cell lung cancer and tumor-associated stroma, Neoplasia 7 (1) (2005) 1–6.

[3] R. Katz-Brull, R. Margalit, P. Bendel, H. Degani, Choline metabolism in breast cancer: ^2H-, ^{13}C- and ^{31}P-NMR studies of cells and tumors, MAGMA 6 (1) (1998) 44–52.

[4] D. Artemov, Z.M. Bhujwalla, U. Pilatus, J.D. Glickson, Two-compartment model for determination of glycolytic rates of solid tumors by in vivo ^{13}C NMR spectroscopy, NMR Biomed. 11 (8) (1998) 395–404.

[5] J.H. Ardenkjaer-Larsen, B. Fridlund, A. Gram, G. Hansson, L. Hansson, M.H. Lerche, R. Servin, M. Thaning, K. Golman, Increase in signal-to-noise ratio of >10,000 times in liquid-state NMR, Proc. Natl. Acad. Sci. USA 100 (18) (2003) 10158–10163.

[6] K. Golman, R.I. Zandt, M. Lerche, R. Pehrson, J.H. Ardenkjaer-Larsen, Metabolic imaging by hyperpolarized ^{13}C magnetic resonance imaging for in vivo tumor diagnosis, Cancer Res. 66 (22) (2006) 10855–10860.

[7] A.P. Chen, M.J. Albers, C.H. Cunningham, S.J. Kohler, Y.F. Yen, R.E. Hurd, J. Tropp, R. Bok, J.M. Pauly, S.J. Nelson, J. Kurhanewicz, D.B. Vigneron, Hyperpolarized C-13 spectroscopic imaging of the TRAMP mouse at 3T-initial experience, Magn. Reson. Med. 58 (6) (2007) 1099–1106.

[8] K. Golman, R. in 't Zandt, M. Thaning, Real-time metabolic imaging, Proc. Natl. Acad. Sci. USA 103 (30) (2006) 11270–11275.

[9] M.J. Albers, R. Bok, A.P. Chen, C.H. Cunningham, M.L. Zierhut, V.Y. Zhang, S.J. Kohler, J. Tropp, R.E. Hurd, Y.F. Yen, S.J. Nelson, D.B. Vigneron, J. Kurhanewicz, Hyperpolarized ^{13}C lactate, pyruvate, and alanine: noninvasive biomarkers for prostate cancer detection and grading, Cancer Res. 68 (20) (2008) 8607–8615.

[10] S.E. Day, M.I. Kettunen, F.A. Gallagher, D.E. Hu, M. Lerche, J. Wolber, K. Golman, J.H. Ardenkjaer-Larsen, K.M. Brindle, Detecting tumor response to treatment using hyperpolarized ^{13}C magnetic resonance imaging and spectroscopy, Nat. Med. 13 (11) (2007) 1382–1387.

[11] O. Warburg, On the origin of cancer cells, Science 123 (3191) (1956) 309–314.

[12] H. Lu, R.A. Forbes, A. Verma, Hypoxia-inducible factor 1 activation by aerobic glycolysis implicates the Warburg effect in carcinogenesis, J. Biol. Chem. 277 (26) (2002) 23111–23115.

[13] W. Dröge, H.P. Eck, H. Kriegbaum, S. Mihm, Release of L-alanine by tumor cells, J. Immunol. 137 (4) (1986) 1383–1386.

[14] L. Brennan, C. Hewage, J.P. Malthouse, G.J. McBean, Gliotoxins disrupt alanine metabolism and glutathione production in C6 glioma cells: a ^{13}C NMR spectroscopic study, Neurochem. Int. 45 (8) (2004) 1155–1165.

[15] S.M. Ronen, A. Volk, J. Mispelter, Comparative NMR study of a differentiated rat hepatoma and its dedifferentiated subclone cultured as spheroids and as implanted tumors, NMR Biomed. 7 (6) (1994) 278–286.

[16] H.R. Harding, F. Rosen, C.A. Nichol, Depression of alanine transaminase activity in the liver of rats bearing walker carcinoma 256, Cancer Res. 24 (1964) 1318–1323.

[17] Cancer Statistics 2008, American Cancer Society. Available from: <http://www.cancer.org/docroot/PRO/content/PRO_1_1_Cancer_Statistics_2008_Presentation.asp>.

[18] J.R. Gingrich, R.J. Barrios, R.A. Morton, B.F. Boyce, F.J. DeMayo, M.J. Finegold, R. Angelopoulou, J.M. Rosen, N.M. Greenberg, Metastatic prostate cancer in a transgenic mouse, Cancer Res. 56 (18) (1996) 4096–4102.

[19] S.J. Kohler, Y. Yen, J. Wolber, A.P. Chen, M.J. Albers, R. Bok, V. Zhang, J. Tropp, S. Nelson, D.B. Vigneron, J. Kurhanewicz, R.E. Hurd, In vivo 13 carbon metabolic imaging at 3T with hyperpolarized ^{13}C-1-pyruvate, Magn. Reson. Med. 58 (1) (2007) 65–69.

[20] A.P. Chen, R.E. Hurd, C.H. Cunningham, Y. Li, M.L. Zierhut, R. Bok, J. Kurhanewicz, S.J. Nelson, D.B. Vigneron, Spatially resolved ^{13}C hyperpolarized dynamic MRS using flyback echo-planar readout trajectory, in: Proceedings 49th Scientific Meeting ENC, Asilomar, CA, 2008, p. 60

[21] C.H. Cunningham, A.P. Chen, M.J. Albers, J. Kurhanewicz, R.E. Hurd, Y.F. Yen, J.M. Pauly, S.J. Nelson, D.B. Vigneron, Double spin-echo sequence for rapid spectroscopic imaging of hyperpolarized ^{13}C, J. Magn. Reson. 187 (2) (2007) 357–362.

[22] C.H. Cunningham, D.B. Vigneron, A.P. Chen, D. Xu, S.J. Nelson, R.E. Hurd, D.A. Kelley, J.M. Pauly, Design of flyback echo-planar readout gradients for magnetic resonance spectroscopic imaging, Magn. Reson. Med. 54 (5) (2005) 1286–1289.

[23] A.P. Chen, J. Kurhanewicz, R. Bok, D. Xu, D. Joun, V. Zhang, S.J. Nelson, R.E. Hurd, D.B. Vigneron, In vivo hyperpolarized ^{13}C MRS/MRSI using ^{13}C-lactate as the pre-polarized substrate, in: Proceedings 16th Scientific Meeting ISMRM, Toronto, Canada, 2008, p. 3192

[24] C.S. Hanes, Studies on plant amylases: the effect of starch concentration upon the velocity of hydrolysis by the amylase of germinated barley, Biochem. J. 26 (5) (1932) 1406–1421.

[25] K.L. Li, X.P. Zhu, A. Jackson, Parametric mapping of scaled fitting error in dynamic susceptibility contrast enhanced MR perfusion imaging, Br. J. Radiol. 73 (869) (2000) 470–481.

[26] K.M. Brindle, I.D. Campbell, R.J. Simpson, A ^1H-NMR study of the activity expressed by lactate dehydrogenase in the human erythrocyte, Eur. J. Biochem. 158 (1986) 299–305.

[27] P.E.Z. Larson, A.B. Kerr, A.P. Chen, M.S. Lustig, M.L. Zierhut, S. Hu, C.H. Cunningham, J.M. Pauly, J. Kurhanewicz, D.B. Vigneron, Multiband excitation pulses for hyperpolarized ^{13}C dynamic chemical shift imaging, J. Magn. Reson. 194 (1) (2008) 121–127.